PCCP

Interfacial Charge Transfer Enhancement via Formation of Binary Molecular Assemblies on Electronically Corrugated Boron Nitride

Journal:	*Physical Chemistry Chemical Physics*
Manuscript ID	CP-ART-09-2019-004853.R1
Article Type:	Paper
Date Submitted by the Author:	14-Nov-2019
Complete List of Authors:	Tan, Andrew; Michigan State University, Physics and Astronomy Zhang, Pengpeng; Michigan State University, Physics and Astronomy

Interfacial Charge Transfer Enhancement via Formation of Binary Molecular Assemblies on Electronically Corrugated Boron Nitride

A.Tan, P. P. Zhang*

Department of Physics and Astronomy, Michigan State University, East Lansing, Michigan 48824-2320, USA

Abstract

Using scanning tunneling microscopy/spectroscopy (STM/STS) in conjunction with finite element simulation, we investigate the interfacial behaviors in single-component zinc phthalocyanine (ZnPc) and hexadecafluorinated zinc phthalocyanine (F_{16}ZnPc) molecular overlayers as well as their 1:1 mixed-phase superstructures on h-BN/Cu(111). We show that the formation of the binary molecular superstructure drastically increases the charge transfer between F_{16}ZnPc molecules and the substrate, which is attributed to the greater electrostatic stability of the binary assembly compared to that of the pure phase. This study highlights the significant complication in the design of donor-acceptor molecular thin films as the presence of the substrate, even a weakly interacting one, such as h-BN/metal, can still perturb the intermolecular charge transfer and thereby the physical behaviors of the hybrid system via interfacial processes.

*corresponding author: zhang@pa.msu.edu

I. Introduction

Studies of interfacial energetics between organic (O) molecules and inorganic (I) substrate, as well as between molecular donor and acceptor identities, have raised enormous interest from both the fundamental perspectives and the technological relevance. These heterointerfaces play a critical role in determining the efficiency of a variety of organic electronic devices such as organic light emitting diodes (OLEDs), organic photovoltaics (OPV), and organic field effect transistors (OFETs).[1-6] Additionally, (bulk) molecular solids of donor-acceptor charge transfer complexes could exhibit rich physical properties with complex phase diagram and/or high carrier mobility originating from the intermolecular charge transfer.[7-11] For thin film applications of this class of material, it is crucial to address the energy level alignment and charge transfer behaviors at the O-O and O-I heterointerfaces. [1, 2, 12-17]

Interfacial energetics and charge transfer behaviors heavily rely on the interactions at the interface.[5, 18-28] For instance, molecular adsorption on a substrate can sometimes lead to hybridization between the frontier molecular orbitals of the adsorbates and the substrate states.[1, 3] This strong molecule-substrate interaction often results in the formation of interface states within the fundamental gap of organic semiconductors and/or the broadening of molecular orbitals, accompanied by a partial or fractional charge transfer with the complex sharing of electrons between molecular adsorbates and the substrate.[1, 3, 27, 29-31] Different models including induced density of interface states (IDIS), induced polarization, and Fermi level pinning by defect/disorder-induced gap (tail) states or localized interface states arising from the formation of chemical bonds have been debated in literature when describing these interfacial phenomena.[1, 3] Concerning donor-acceptor binary superstructures particularly, hybridization occurring at the strongly interacting molecule-substrate interface could perturb the pristine molecular orbitals and further dominate the characteristics of the molecular systems.[32]

Recently, understanding of the charge transfer behaviors between molecular adsorbates and weakly interacting substrates has been significantly advanced. [3, 12, 25, 27, 31, 33-44] In contrast to strongly interacting systems, charge transfer, if it occurs, is via the tunneling mechanism and the transferred charges are in integer quantities, i.e., integer charge transfer (ICT).[25, 27, 31, 43, 44] One of the more recent interpretations of the ICT model is based on the concept of the dynamic coexistence of charged and neutral molecules within the molecular overlayer, which is supported by experimental observations from x-ray photoelectron spectroscopy (XPS) and ultraviolet photoemission spectroscopy (UPS). [12, 31, 40-42] The electrostatics of the system plays a critical role in determining the percentage of charged molecules in the film, where the charge state of each individual molecule is strongly dependent on the arrangement of neighboring molecules at any given moment in time.[31]

Despite the progress in the refinement of the ICT model, much less is known about the charge transfer behaviors and the associated electrostatics in complex systems consisting of donor-acceptor binary molecular superstructures and weakly interacting substrates. As discussed earlier,

intermolecular charge transfer between donor and acceptor molecular moieties can give rise to intriguing electronic or correlated phases in binary systems in the bulk form. Nevertheless, in thin films or self-assembled monolayers, how the interfacial charge transfer influences the intermolecular charge transfer or vice versa, along with the energy level alignment at the interfaces, are anticipated to have profound impacts on the properties of heterostructures even on weakly interacting substrates.[13, 32, 45-52]

In this work, using scanning tunneling microscopy/spectroscopy (STM/STS) and finite element analysis, we investigate the charge transfer behavior and interfacial energetics in molecular structures composed of zinc phthalocyanine (ZnPc) and its fluorinated counterpart, hexadecafluorinated zinc phthalocyanine (F_{16}ZnPc), on monolayer hexagonal boron nitride (h-BN) grown on Cu(111). Due to its insulating nature, h-BN serves to decouple the molecular overlayer from the metallic substrate, which prevents strong hybridization at the interface and confines the system to the ICT regime.[53-57] ZnPc and F_{16}ZnPc are chosen as the donor and acceptor molecular species of interest due to their geometric similarity, the inert metal center which further reduces possible interaction pathways with the substrate, and their predicted ability to exhibit donor-acceptor intermolecular charge transfer characteristics when packed edge-to-edge. We show that these two molecules can both form weakly interacting self-assembled structures on h-BN/Cu(111) surface with minimal interfacial charge transfer, and the co-deposition of the two molecular species onto the substrate yields a checkerboard binary superstructure that is adopted to minimize the F-F repulsion between F_{16}ZnPc molecules. In comparison to those of the pure phases, the electronic structure of F_{16}ZnPc in the binary system is shifted down in energy, whereas the energy levels of ZnPc are upshifted toward the vacuum level. This observation is attributed to the formation of interface dipoles arising from the enhanced charge transfer between the F_{16}ZnPc constituents and the substrate in the binary blend, which leads to an overall vacuum level shift of the entire molecular layer. In conjunction with the finite element analysis, we speculate that the increased charge transfer interaction originates from the greater Madelung energy analog of the binary superstructure, which stabilizes the charged F_{16}ZnPc molecules against the intermolecular coulomb repulsion. This study contributes to a better understanding of the charge transfer processes in donor-acceptor molecular superstructures in the presence of a weakly interacting substrate.

II. Experimental Details

Experiments were carried out in an ultrahigh vacuum (UHV) setup, using a commercial LT-Omicron scanning microscope operated at 77K. STM images were taken at constant current mode with a Pt-Ir tip. STS acquisition was achieved with the lock-in technique. Typical modulation bias and frequency were 26 mV and 1 kHz, respectively. Spectra on Ag(111) were taken periodically as a reference to confirm tip consistency. The Cu(111) surface was cleaned by repeated ion sputter cycles at 2keV, ~30uA. The h-BN layer was grown via a UHV-chemical vapor deposition process using borazine, produced by the thermal decomposition of ammonia borane, as the precursor. Borazine gas was then flowed onto the Cu(111) surface via a leak valve at a pressure

of ~1 × 10^{-6} mbar. The substrate was held at ~820°C during the h-BN growth. This growth is a self-limiting process since the catalytic activity of Cu(111) is drastically reduced once the surface is passivated by a complete h-BN monolayer.[58] ZnPc and F_{16}ZnPc were purified by sublimation processes before being loaded into the UHV system. The molecules were then degassed prior to use. ZnPc and F_{16}ZnPc monolayers were grown by thermal evaporation, while the mixed-phase binary superstructure was grown by the co-deposition of both molecules from separate sources. The substrate was held between room temperature and 150°C during the deposition of molecular species.

Finite element analysis was conducted in COMSOL. The Cu substrate and free space were defined as 1 um × 1 um × 1 um cubes. The potential at the outer boundaries of the system was set to 0 V. The dielectric constants used for the materials are as follows: h-BN (3.29), molecules (5) and Cu (>100).[59-61] The image plane position of the Cu(111) substrate was allowed to extend an angstrom above the metal surface.[62-64] The thickness of the molecular layer is approximately two times of the van der Waals binding distance (0.3 nm) to account for the protruding π-orbital into the vacuum, with the h-BN thickness being the Cu-BN interlayer distance.[65] The size of the molecules was approximated by the size of the molecular unit cell in the single-component pure layers (1.44 nm × 1.44 nm). When individual molecules were charged initially, a uniform charge density was employed without considering the detailed internal charge distribution within molecules.

III. Results and Discussion

Self-assembly of single-component or binary molecular monolayers on the surface of a clean metal has been extensively explored in the past. [32, 43, 45-51, 66, 67] As discussed previously, often, chemical interaction with the formation of chemical bonds or weak hybridization between molecular orbitals and the continuum states of the metallic substrate emerges at the hetero-interface, leading to the complex sharing of electrons and/or hybridized interface states which can dominate the characteristics of molecular thin films. [1, 31, 32, 43, 66, 68, 69] Furthermore, the 'push-back' or Pauli repulsion effect where the electron tails of the clean metal surface are pushed back into the metal by molecular adsorbates effectively reducing the metal work function and thus modulates the positions of the frontier molecular orbitals relative to the substrate Fermi level.[1, 3, 70] Since the 'push-back' effect is highly sensitive to the adsorption height of molecular adsorbates, any perturbation of the height or the charge reorganization in the binary molecular blend is expected to notably modify the interfacial energy level alignment.[48] Thus, to confine the system to the weakly interacting regime and to largely preserve the intrinsic properties of molecular structures, a decoupling layer will be desirable. Inorganic salts and 2D materials, such as sodium chloride, has been exploited for this purpose.[31, 49, 71] More recently, h-BN monolayer has also demonstrated its capabilities in decoupling molecular adsorbates from the metallic substrate, yet it offers the additional advantage of imposing periodic electronic modulations to the molecular overlayer through Moiré patterns.[53-56, 72, 73]

Figure 1a shows the Moiré pattern of h-BN on Cu(111), which is hexagonal in nature but the exact periodicity of the pattern depends on the specific azimuthal rotation of the h-BN domain with respect to the Cu(111) surface.[55, 56] The growth of molecular species on h-BN/Cu(111) proceeds with preferential nucleation on the 'hill' locations of the Moiré pattern at low coverage, which eventually expands outwards to form a molecular overlayer (Fig. S1). Figure 1b-d show the zoomed in STM images of the single-component ZnPc assembly, F_{16}ZnPc assembly, and the ZnPc-F_{16}ZnPc binary blend, respectively. In the binary superstructure, molecules adopt a checkerboard pattern where F_{16}ZnPc occupy alternating sites within the ZnPc lattice. This geometric configuration arises from the hydrogen bonding interaction between ZnPc and F_{16}ZnPc molecules, which also suppresses the F-F repulsion between F_{16}ZnPc molecules as compared to that of the pure F_{16}ZnPc film (see Fig. S1 and the associated discussion in the Supplemental Material). Like the single-component molecular layers, packing within the binary superstructure is not perturbed by the h-BN/Cu(111) Moiré patterns that are geometrically flat. Note that the origin of the STM contrast in Fig. 1a is not the morphology corrugation, but instead an electronic effect.[53, 55, 56, 72, 73]

While molecular packing is relatively uniform across the surface, electronic variations due to the Moiré perturbation can be observed across all three assemblies (Fig. S2). Figure 2a shows the STS spectra taken on the ZnPc monolayer, F_{16}ZnPc monolayer, and above the ZnPc and F_{16}ZnPc constituents within the binary superstructure, respectively. In all these spectra, well-defined density of states (DOS) features at positive bias are identified. Gaussian deconvolution of these DOS features (Fig. S3) reveals molecular peaks associated with the lowest unoccupied molecular orbitals (LUMOs), as evidenced by the pristine molecular orbital-like features observed in both the STM images and the differential conductance maps taken at the corresponding biases (Fig. 1b-d and Fig. S1-2), accompanied by additional vibronic satellites.[13, 74-78] The existence of the negative differential resistance (NDR) regime following the DOS features further proves the weak interaction between the molecular overlayers and the substrate, suggesting that h-BN has functioned as a decoupling layer which effectively suppresses the hybridization between molecular moieties and the Cu(111) substrate. Nevertheless, when the spectra taken on the hill and valley locations of the Moiré pattern are compared within each individual assembly, ~0.25eV difference in the onset of the DOS feature can be depicted. This is in agreement with the expected local work function modulation arising from the Moiré pattern of the h-BN/Cu(111) substrate, which correspondingly perturbs the positions of the frontier molecular orbitals with respect to the substrate Fermi level.[53, 54]

Theoretical calculations of the CuPc-F_{16}CuPc heterostructure, a close approximation to the ZnPc variant, suggests the existence of intermolecular charge transfer when donor and acceptor molecules are packed side-to-side.[37] Consequently, the local vacuum level above the positively/negatively charged donor/acceptor molecular identities is expected to shift with respect to that exhibited in the single-component pure layers, leading to the LUMO of the donor shifting closer to the substrate Fermi level whereas the LUMO of acceptor, further away.[3, 79] Nevertheless, our STS data taken on the binary superstructure illustrate a different picture: ZnPc molecular

orbitals are consistently observed at higher energies (by up to ~0.5V) relative to the substrate Fermi level as compared to that of the pure layer, while the F_{16}ZnPc positive peak feature has migrated even closer to the Fermi level (Fig. 2a). This observation indicates that the intermolecular charge transfer either does not exist or does not play a dominant role in the energy level alignment of the binary superstructure on h-BN/Cu(111). It is worth noting that Moiré pattern of the substrate simply serves as a work function modulating template, which does not seem to alter the baseline behavior of the donor-acceptor binary blend (as shown in Fig. S2). As a result, we focus the discussion using the representative STS spectra taken on the valley sites of the substrate.

Similar trend of orbital shifts with respect to the single-component pure layers has been observed in various donor-acceptor binary blends adsorbed on clean metal substrates.[32, 45-51] This has been largely attributed to the Pauli repulsion effects coupled with perturbations of the adsorption height of each molecular constituents and the involved charge reorganization in the binary blend, as discussed earlier.[45, 48, 50, 51] In these studies, it was assumed that the induced density of interface states arising from the (weak) hybridization of molecular adsorbates and the metal substrate are positioned away from the Fermi level, thus not contributing significantly to the interfacial energy level alignment. Nonetheless, the Pauli repulsion effects should have been greatly suppressed by the h-BN decoupling layer in our studies.[62] Furthermore, different from the ensemble-averaged UPS and core-level x-ray photoelectron spectroscopy (XPS) techniques where the donor-acceptor ratio dictates the averaged work function of the blend, STS exploited in this study is a local probe technique. Thus, the opposite shifts of the donor and acceptor molecular orbitals with respect to the substrate Fermi level owing to the work function averaging can be minimized.[48, 51, 80]

Other factors that could possibly impact the positions of the molecular orbitals in the binary donor-acceptor blend as compared to the pure layers include i) intermolecular hybridization and charge redistribution via formation of hydrogen bonding between ZnPc and F_{16}ZnPc, ii) electrostatic screening by the supramolecular environment, and iii) interfacial (integer) charge transfer.[4, 13, 45-49] As shown in Fig. 1d, pristine looking molecular orbitals of F_{16}ZnPc is exhibited in the binary blend, indicating that no significant hybridization has occurred between the donor and acceptor molecules. Regarding the electrostatic screening by neighboring molecules, if we assume that ZnPc and F_{16}ZnPc molecules have comparable polarizabilities, each individual donor or acceptor molecule should experience similar degree of screening within the pure and the binary blend owing to the same coordination number and the similar intermolecular distance (see detailed discussion in Section 4 of the Supplemental Material).[13, 59, 60] With these considerations, we focus the following discussion on interfacial charge transfer and the associated interfacial behaviors in the single-component molecular overlayers as well as the binary blend. Note that van der Waals interactions between molecules and molecule-substrate results in the suppression of strain-related effects as typically exhibited in atomic heterojunctions composed of inorganic materials.[81-83]

A comparison of the LUMO energy level of the ZnPc monolayer revealed in our STS measurements with those derived from the literature reported molecular electron affinity (EA) and

work function of h-BN/Cu(111) suggests that ZnPc on h-BN/Cu(111) is vacuum level aligned and that charge transfer between the molecular adsorbates and the substrate is minimal as seen in Fig. 2b. The case of F_{16}ZnPc molecular overlayer is a bit more puzzling. Due to the more electronegative nature of F_{16}ZnPc, its LUMO is expected to sit ~0.5eV closer to the substrate Fermi level than that of ZnPc.[84] Although this trend is observed in our experiment, the difference between the ZnPc and F_{16}ZnPc LUMO peak positions (~0.2eV) is much smaller, suggesting that a finite amount of charge has been transferred into the F_{16}ZnPc LUMO which results in the formation of an interface dipole that shifts the vacuum level and the F_{16}ZnPc LUMO away from the substrate Fermi level by ~0.3eV (Fig. 2b). To estimate the size of the interfacial charge transfer between F_{16}ZnPc and the substrate, finite element electrostatics simulations (Fig. S5a) were conducted using the COMSOL program. The structure is set up as shown in Fig. 3a. In this simple model, all F_{16}ZnPc molecules are charged with a uniform charge density, and the degree of charge transfer is fine-tuned to match the upshift of its LUMO (~0.3eV) extrapolated from the experimental observation. This yields a ~0.27e charge transfer per molecule. This charging process increases the electrostatic potential energy of electrons above the molecular adsorbates, thereby shifting the vacuum level, and correspondingly the LUMO orbitals, upwards. It should be noted that in weakly interacting physisorbed systems, such as the case of F_{16}ZnPc on h-BN, interfacial charge transfer is mediated via electron tunneling between molecular orbitals and substrate states. As discussed previously, this process is generally described by the ICT model, where the dynamic coexistence of charged and neutral molecules often render the average amount of charge transfer per molecule fractional.[31, 40] In this case, it can be expected that at any instance of time, one out of every four F_{16}ZnPc molecules is charged.

Upon understanding the interfacial behavior in singe-component molecular overlayers, we revisit the binary superstructure. The upshift of the ZnPc LUMO observed in the binary blend as compared to the pure layer (Fig. 2a-b) could be a direct consequence of the overall negatively charged film via interfacial charge transfer. However, it is unlikely that ZnPc becomes charged while F_{16}ZnPc, a more electronegative molecule that has already been demonstrated to charge transfer with the substrate, remains charge neutral. This leads us to hypothesize that F_{16}ZnPc molecules in the binary blend have charge transferred with the substrate more than what was suggested in the pure layer, and the resulting interfacial dipole is responsible for the observed upshift in the ZnPc LUMO. To verify this hypothesis, the system is, once again, recreated in COMSOL (see detailed discussion of COMSOL simulation in Section 6 of the Supplemental Material). In this model, F_{16}ZnPc molecules are charged in a checkerboard pattern that approximates the binary superstructure where the ZnPc molecules occupy every other site and remain neutral (Fig. 3b). The electrostatic potential energy of electrons above the molecular adsorbates, specifically ZnPc, is calculated and the amount of charge transferred between F_{16}ZnPc molecules and the substrate is tuned to match the ~0.5eV upshift of the ZnPc LUMO in the binary blend. Based on these parameters, we find that a ~1e charge transfer is required to produce a similar magnitude upshift, as seen in Fig. 3c. The population of the F_{16}ZnPc LUMO explains the shift of this orbital towards the Fermi level in the blend. It should be noted that the 1e occupation and

weakly interacting nature of F_{16}ZnPc on h-BN/Cu(111) system could lead to a splitting of the molecule's LUMO into its corresponding singly unoccupied and singly occupied molecular orbitals SUMO/SOMO (See Section 5 of the Supplemental Material for more detailed discussion). Further refinement could be done by adjusting the image plane position of the Cu(111) surface.[62-64]

This now defines a clear difference in regime between the charging behavior of F_{16}ZnPc in its pure layer, where charge transfer is fractional and dynamic, and in the ZnPc/F_{16}ZnPc binary blend, where the charging is complete and static. An intriguing question remains to be addressed, i.e., why F_{16}ZnPc molecules charge more in the binary superstructure than in its pure layer. In the ICT model involving interfaces between organic molecules and inorganic substrates, charge transfer can typically be categorized into three separate regimes.[3, 4, 31, 37] Two of these regimes are straightforward where the LUMO of molecular adsorbates either sits very far above the Fermi level of the substrate, thereby prohibiting direct interfacial charge transfer, or far beneath the Fermi level where the charge transfer is strongly favored. The third regime is when the LUMO lies slightly above the Fermi level of the substrate, typically within ~0.5eV from E_F.[1, 37] Interfacial charge transfer has been demonstrated in this scenario, and different mechanisms including Fermi level pinning by polaron states associated with the nuclear relaxation of charged molecules or as a natural consequence of the Fermi-Dirac statistics coupled with the DOS distribution of organic molecular systems, particularly, the tail states that extend into the molecular gap, have been proposed.[3, 85, 86] Nevertheless, the relaxation energy in conjugated small organic molecules are typically much smaller than 0.5eV, and DOS broadening, relating to imperfect molecular structures, may not be the main reason for the enhanced interfacial charge transfer due to the comparable degrees of molecular ordering exhibited in the pure layer and the binary blend as well as the localized nature of the STM probing.[1, 36]

We speculate that the interfacial charge transfer can be enabled/enhanced in molecular assemblies when the resulting electrostatic energy of the system consisting of the charged molecular lattice and the substrate is sufficient to compensate for the LUMO-Fermi level offset. The electrostatic energy of the system is the sum-total of the two separate energy terms, i.e., the stabilizing energy between the charged molecules and their corresponding image charges in the substrate, typically known as the polarization energy, and the destabilizing energy between adjacent charged molecules. This sum-total electrostatic energy in the molecular overlayer on h-BN/Cu(111) is analogous to the Madelung energy, i.e., the energy gained by the formation of an ionic matrix from its charged constituents, in organic charge transfer complexes or ionic systems (see detailed discussion of Madelung energy in Section 6 of the Supplemental Material). [7-9] Therefore, for ease of discussion, it is referred to as, simply, the Madelung energy in the following analysis.

Considering the binary system, ZnPc molecules do not appear to directly interact with the F_{16}ZnPc molecules, therefore their role within this estimation of the Madelung energy is simply that of a dielectric spacer. In this context, the Madelung energy of the binary blend is anticipated to be larger than that of the pure system due to the weaker electron-electron repulsion between the

more widely spaced charged F_{16}ZnPc molecules. To provide a quantitative estimation, we calculate the Madelung energy per F_{16}ZnPc molecule in the binary assembly and in its pure layer. As just discussed, to first approximation, this energy can be described by the equation $M = P - E_{ee}$ where P is the polarization energy and E_{ee} is the destabilizing energy arising from the e-e repulsion.[87, 88] The polarization energy is calculated by taking the difference between the charging energy of a molecule in free space and within the system with the molecular layer treated as continuum dielectric medium (Fig. S6).[89] P amounts to 0.78eV in both the binary blend and the pure layer, whereas the destabilizing energy acting on individual F_{16}ZnPc molecules should differ between the two systems due to the stronger e-e repulsion involved in the latter. This destabilizing energy can be estimated in a matrix with the F_{16}ZnPc molecules either charged in a checkerboard pattern (inset of Fig. 3(c)) mimicking the binary blend or on every molecular site for the pure layer. In comparison to the model system consisting of continuum molecular dielectric layers, the additional electrostatic energy associated with charging a molecule in the charged matrix is, therefore, E_{ee}, which amounts to 0.07 eV and 0.27 eV in the checkerboard and fully charged matrix, respectively (See Fig. S6 in the Supplemental Material for a schematic diagram illustrating these scenarios). Thus, the Madelung energy is approximated to be 0.71 eV for the binary superstructure and 0.51 eV for the pure layer. The larger Madelung energy provides a greater driving force for interfacial charge transfer to occur, which lends quantitative evidence to the more negatively charged binary blend as opposed to the pure layer.

IV. Conclusion

In conclusion, we have demonstrated that ZnPc and F_{16}ZnPc, in their pure phase, form weakly interacting organized structures that are electronically but not geometrically perturbed by the Moiré patterns of the h-BN/Cu(111) substrate. Co-deposition of these two molecules yields a checkerboard binary superstructure that is adopted to minimize the F-F repulsion between F_{16}ZnPc molecules. The energy levels of molecular orbitals in the binary blend are observed to upshift for ZnPc and downshift for F_{16}ZnPc with respect to those of the pure phase, regardless of the location of the h-BN Moiré pattern. This trend is opposite to that expected if donor-acceptor intermolecular charge transfer has dominated. Instead, it is the result of the enhanced charging of F_{16}ZnPc molecules in the binary blend via interfacial charge transfer with the substrate. The emergence of this charge transfer interaction is hypothesized to originate from the greater Madelung energy analog of the binary superstructure in contrast to that of the pure phase. This phenomenon brings forth a significant complication as well as a great opportunity in the design of donor-acceptor molecular thin films as the presence of the substrate, even a weakly interacting one, such as h-BN/metal that does not perturb the pristine molecular orbitals and characteristics, can still promote interfacial charge transfer and inhibit intermolecular charge transfer. On one hand, steps will need to be taken to further decouple these molecular structures from the substrate to keep their intrinsic properties. On the other hand, interfacial charge transfer may act as an additional knob to engineer the properties of donor-acceptor molecular thin films which could enrich the potential (opto)electronic applications of the hybrid system.

Conflicts of Interest

There are no conflicts of interest to declare.

Acknowledgments

We acknowledge the financial support from the U.S. Department of Energy (DOE), Office of Basic Energy Sciences, Division of Materials Sciences and Engineering under Award Number DE-SC0019120. We also acknowledge Sahar Sharifzadeh for helpful discussions on finite element simulation.

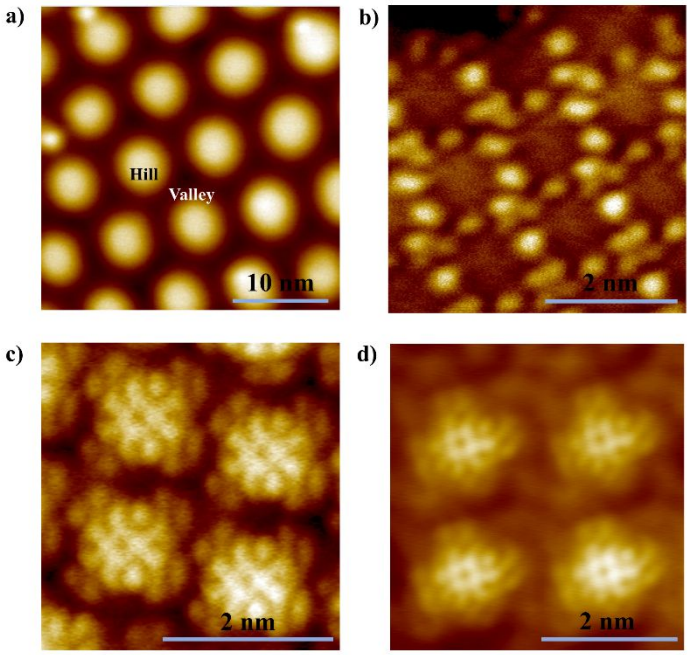

Figure 1: STM topography images taken on (a) h-BN/Cu(111) with the hill and valley locations of the Moiré pattern labelled (V_s = 4 V, I_t = 2 pA), (b) ZnPc monolayer (V_s = -2 V, I_t = 3 pA), (c) F_{16}ZnPc monolayer (V_s = 2 V, I_t = 2 pA), and (d) ZnPc/F_{16}ZnPc binary blend (V_s = 0.15 V, I_t = 75 pA) on h-BN/Cu(111). Pristine molecular orbital-like features are observed, demonstrating the weak interaction between the organic molecules and the underlying h-BN/Cu(111) substrate. The lattice parameters of the molecular overlayers are listed in Table S1.

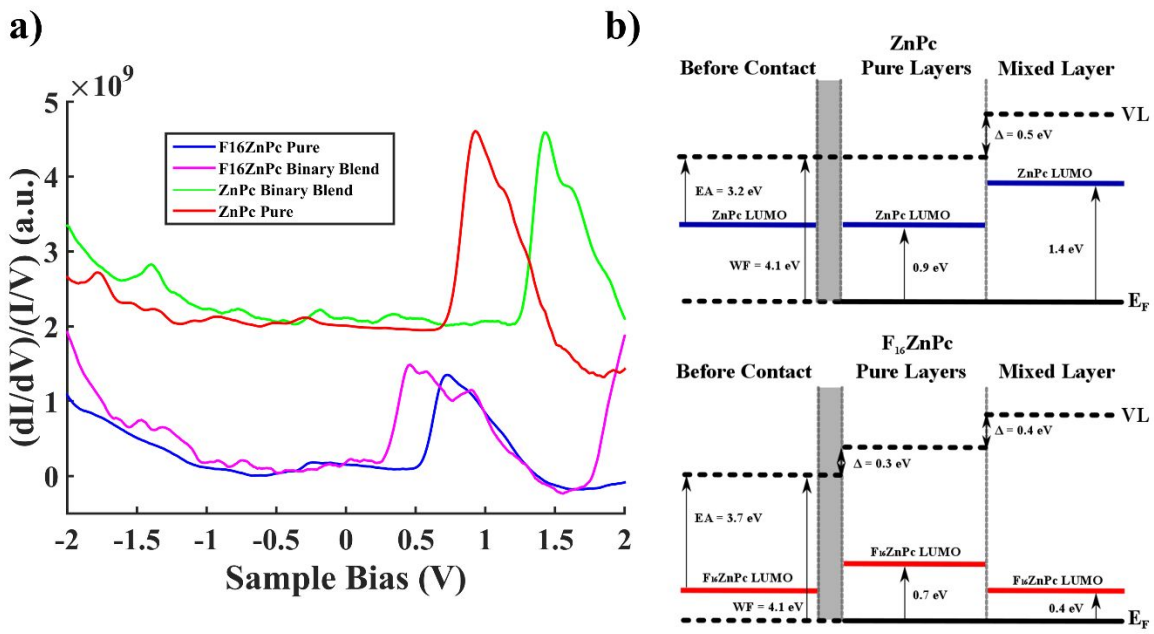

Figure 2: (a) STS taken on valley locations of the pure ZnPc (setpoint: V_s = 2V, I_t = 100pA), pure F_{16}ZnPc (V_s = 2V, I_t = 50pA), and on the ZnPc/F_{16}ZnPc constituents in the mixed binary blend (V_s = 2V, I_t = 100pA). (b) Energy-level alignment diagrams for ZnPc (top) and F_{16}ZnPc (bottom) in the pure layer and mixed binary blend at valley locations of the h-BN/Cu(111) substrate. Literature reported values of the molecular electron affinity (EA: molecular LUMO with respect to the vacuum level) and the work function of h-BN/Cu(111) valley areas (WF: Fermi level with respect to the vacuum level) are labelled in the "Before Contact" regime. [53, 84] Upon contact, charge transfer may occur at the interface which shifts the vacuum level (VL) as well as the positions of molecular orbitals relative to the substrate Fermi level (E_F). Gaussian-fit peak positions of the LUMO features in (a) are listed in Table S1.

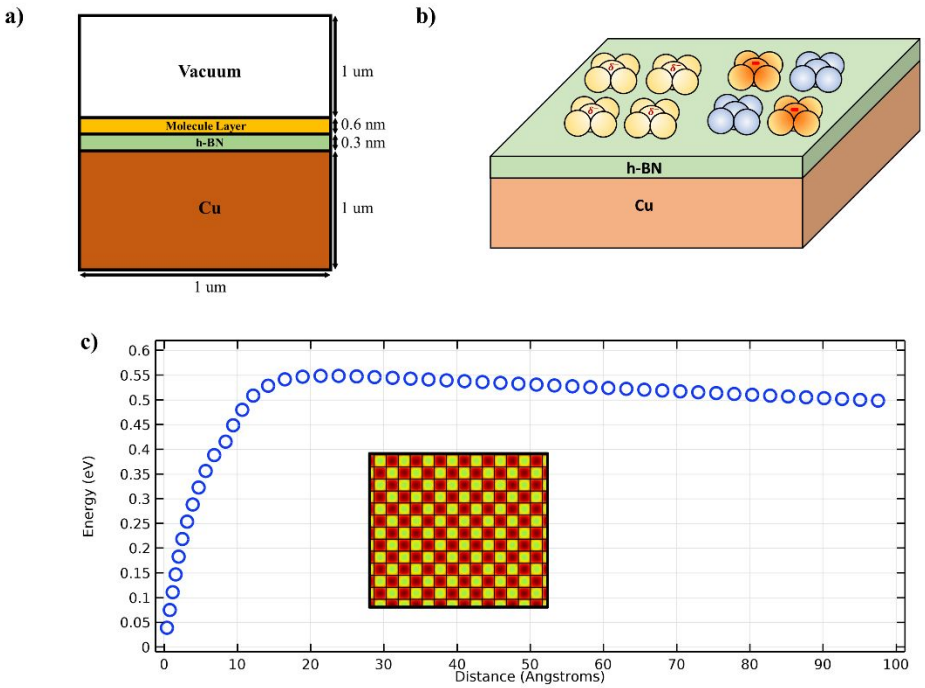

Figure 3: Finite element electrostatic simulations using COMSOL. (a) 2D representation of the geometric setup of the simulation. (b) Schematic illustration of the charge state of F_{16}ZnPc molecules in its pure layer (left) and the mixed binary blend (right), respectively. (c) Electrostatic potential energy for electrons is plotted from the image charge plane of the metal up to 100 angstroms directly above the ZnPc molecule near the center of the binary molecular assembly. The potential energy for electrons reaches the maximum a couple of nanometers beyond the image charge plane, corresponding to the upshift of the local vacuum level (above the ZnPc constituents), which then decays to a saturation value with increasing distance. Inset shows a portion of the 100 × 100 checkerboard matrix used in the calculation, where F_{16}ZnPc molecules are charged by 1e (red) and ZnPc remain neutral (yellow).

References:

1. J. Hwang, A. Wan and A. Kahn, *Materials Science and Engineering: R: Reports*, 2009, **64**, 1-31.
2. D. Cahen, A. Kahn and E. Umbach, *Materials Today*, 2005, **8**, 32-41.
3. S. Braun, W. R. Salaneck and M. Fahlman, *Advanced Materials*, 2009, **21**, 1450-1472.
4. S. Braun, W. Osikowicz, Y. Wang and W. R. Salaneck, *Organic Electronics*, 2007, **8**, 14-20.
5. F. Bussolotti, J. Yang, A. Hinderhofer, Y. Huang, W. Chen, S. Kera, A. T. S. Wee and N. Ueno, *Phys. Rev. B*, 2014, **89**, 115319.
6. H. Ishii, K. Sugiyama, E. Ito and K. Seki, *Advanced Materials*, 1999, **11**, 605.
7. J. B. Torrance, *Annals of the New York Academy of Sciences*, 1978, **313**, 210-233.
8. G. Saito and Y. Yoshida, *Top Curr Chem*, 2012, **312**, 67-126.
9. K. P. Goetz, D. Vermeulen, M. E. Payne, C. Kloc, L. E. McNeil and O. D. Jurchescu, *J. Mater. Chem. C*, 2014, **2**, 3065-3076.
10. J.-P. Pouget, P. Alemany and E. Canadell, *Materials Horizons*, 2018, **5**, 590-640.
11. R. Rösslhuber, E. Rose, T. Ivek, A. Pustogow, T. Breier, M. Geiger, K. Schrem, G. Untereiner and M. Dressel, *Crystals*, 2018, **8**, 121.
12. A. Della Pia, M. Riello, A. Floris, D. Stassen, T. S. Jones, D. Bonifazi, A. De Vita and G. Costantini, *ACS Nano*, 2014, **8**, 12356-12364.
13. J. Q. Zhong, X. Qin, J. L. Zhang, S. Kera, N. Ueno, A. T. Wee, J. Yang and W. Chen, *ACS Nano*, 2014, **8**, 1699-1707.
14. W. Gao and A. Kahn, *Organic Electronics*, 2002, **3**, 53-63.
15. F. Jackel, U. G. Perera, V. Iancu, K. F. Braun, N. Koch, J. P. Rabe and S. W. Hla, *Physical Review Letters*, 2008, **100**, 126102.
16. W. H. Soe, C. Manzano, H. S. Wong and C. Joachim, *J Phys Condens Matter*, 2012, **24**, 354011.
17. T. R. Umbach, I. Fernandez-Torrente, J. N. Ladenthin, J. I. Pascual and K. J. Franke, *J Phys Condens Matter*, 2012, **24**, 354003.
18. I. Avilov, V. Geskin and J. Cornil, *Adv Funct Mater*, 2009, **19**, 624-633.
19. M. Linares, D. Beljonne, J. Cornil, K. Lancaster, J. L. Bredas, S. Verlaak, A. Mityashin, P. Heremans, A. Fuchs, C. Lennartz, J. Ide, R. Mereau, P. Aurel, L. Ducasse and F. Castet, *J Phys Chem C*, 2010, **114**, 3215-3224.
20. J. B. Neaton, M. S. Hybertsen and S. G. Louie, *Physical Review Letters*, 2006, **97**, 216405.
21. S. Verlaak, D. Beljonne, D. Cheyns, C. Rolin, M. Linares, F. Castet, J. Cornil and P. Heremans, *Adv Funct Mater*, 2009, **19**, 3809-3814.
22. S. R. Yost, L. P. Wang and T. Van Voorhis, *J Phys Chem C*, 2011, **115**, 14431-14436.
23. K. J. Franke, G. Schulze, N. Henningsen, I. Fernandez-Torrente, J. I. Pascual, S. Zarwell, K. Ruck-Braun, M. Cobian and N. Lorente, *Physical Review Letters*

2008, **100**, 036807.

24. I. Fernández Torrente, K. J. Franke and J. Ignacio Pascual, *Journal of Physics: Condensed Matter*, 2008, **20**, 184001.
25. X. Lu, M. Grobis, K. H. Khoo, S. G. Louie and M. F. Crommie, *Phys. Rev. B*, 2004, **70**, 115418.

26. J. D. Sau, J. B. Neaton, H. J. Choi, S. G. Louie and M. L. Cohen, *Physical Review Letters*, 2008, **101**, 026804.
27. A. Mugarza, R. Robles, C. Krull, R. Korytár, N. Lorente and P. Gambardella, *Phys. Rev. B*, 2012, **85**, 155437.
28. A. Tan, S. R. Wagner and P. P. Zhang, *Phys. Rev. B*, 2017, **96**, 035313.
29. M. N. Faraggi, N. Jiang, N. Gonzalez-Lakunza, A. Langner, S. Stepanow, K. Kern and A. Arnau, *J Phys Chem C*, 2012, **116**, 24558-24565.
30. F. S. Tautz, M. Eremtchenko, J. A. Schaefer, M. Sokolowski, V. Shklover and E. Umbach, *Phys. Rev. B*, 2002, **65**, 125405.
31. O. T. Hofmann, P. Rinke, M. Scheffler and G. Heimel, *ACS Nano*, 2015, **9**, 5391-5404.
32. N. Gonzalez-Lakunza, I. Fernandez-Torrente, K. J. Franke, N. Lorente, A. Arnau and J. I. Pascual, *Phys Rev Lett*, 2008, **100**, 156805.
33. M. T. Greiner, M. G. Helander, W. M. Tang, Z. B. Wang, J. Qiu and Z. H. Lu, *Nat Mater*, 2011, **11**, 76-81.
34. L. Ley, Y. Smets, C. I. Pakes and J. Ristein, *Adv Funct Mater*, 2013, **23**, 794-805.
35. J.-P. Yang, L.-T. Shang, F. Bussolotti, L.-W. Cheng, W.-Q. Wang, X.-H. Zeng, S. Kera, Y.-Q. Li, J.-X. Tang and N. Ueno, *Organic Electronics*, 2017, **48**, 172-178.
36. M. Oehzelt, N. Koch and G. Heimel, *Nat Commun*, 2014, **5**, 4174.
37. D. Çakir, M. Bokdam, M. P. de Jong, M. Fahlman and G. Brocks, *Applied Physics Letters*, 2012, **100**, 203302.
38. Y.-Y. Du, W.-J. Li, G.-H. Chen, D.-Q. Lin, L.-X. Wang, R. Wu, J.-O. Wang, H.-J. Qian, K. Ibrahim and H.-N. Li, *AIP Advances*, 2019, **9**, 045122
39. Q. Bao, S. Fabiano, M. Andersson, S. Braun, Z. Sun, X. Crispin, M. Berggren, X. Liu and M. Fahlman, *Adv Funct Mater*, 2016, **26**, 1077-1084.
40. P. Amsalem, J. Niederhausen, A. Wilke, G. Heimel, R. Schlesinger, S. Winkler, A. Vollmer, J. P. Rabe and N. Koch, *Phys. Rev. B*, 2013, **87**, 035440.
41. S. Winkler, P. Amsalem, J. Frisch, M. Oehzelt, G. Heimel and N. Koch, *Materials Horizons*, 2015, **2**, 427-433.
42. H. Wang, P. Amsalem, G. Heimel, I. Salzmann, N. Koch and M. Oehzelt, *Adv Mater*, 2014, **26**, 925-930.
43. M. Toader, T. G. Gopakumar, P. Shukrynau and M. Hietschold, *J Phys Chem C*, 2010, **114**, 21548-21554.
44. S.-A. Savu, G. Biddau, L. Pardini, R. Bula, H. F. Bettinger, C. Draxl, T. Chassé and M. B. Casu, *J Phys Chem C*, 2015, **119**, 12538-12544.
45. A. El-Sayed, P. Borghetti, E. Goiri, C. Rogero, L. Floreano, G. Lovat, D. J. Mowbray, J. L. Cabellos, Y. Wakayama, A. Rubio, J. E. Ortega and D. G. de Oteyza, *ACS Nano*, 2013, **7**, 6914-6920.
46. N. Gonzalez-Lakunza, M. E. Canas-Ventura, P. Ruffieux, R. Rieger, K. Mullen, R. Fasel and A. Arnau, *Chemphyschem*, 2009, **10**, 2943-2946.
47. J. L. Cabellos, D. J. Mowbray, E. Goiri, A. El-Sayed, L. Floreano, D. G. de Oteyza, C. Rogero, J. E. Ortega and A. Rubio, *J Phys Chem C*, 2012, **116**, 17991-18001.
48. E. Goiri, P. Borghetti, A. El-Sayed, J. E. Ortega and D. G. de Oteyza, *Adv Mater*, 2016, **28**, 1340-1368.
49. K. A. Cochrane, T. S. Roussy, B. Yuan, G. Tom, E. Mårsell and S. A. Burke, *J Phys Chem C*, 2018, **122**, 8437-8444.

50. B. Stadtmuller, D. Luftner, M. Willenbockel, E. M. Reinisch, T. Sueyoshi, G. Koller, S. Soubatch, M. G. Ramsey, P. Puschnig, F. S. Tautz and C. Kumpf, *Nat Commun*, 2014, **5**, 3685.
51. J. Rodríguez-Fernández, M. Robledo, K. Lauwaet, A. Martín-Jiménez, B. Cirera, F. Calleja, S. Díaz-Tendero, M. Alcamí, L. Floreano, M. Domínguez-Rivera, A. L. Vázquez de Parga, D. Écija, J. M. Gallego, R. Miranda, F. Martín and R. Otero, *J Phys Chem C*, 2017, **121**, 23505-23510.
52. G. D'Avino, L. Muccioli, F. Castet, C. Poelking, D. Andrienko, Z. G. Soos, J. Cornil and D. Beljonne, *J Phys Condens Matter*, 2016, **28**, 433002.
53. S. Joshi, D. Ecija, R. Koitz, M. Iannuzzi, A. P. Seitsonen, J. Hutter, H. Sachdev, S. Vijayaraghavan, F. Bischoff, K. Seufert, J. V. Barth and W. Auwarter, *Nano Lett*, 2012, **12**, 5821-5828.
54. S. Joshi, F. Bischoff, R. Koitz, D. Ecija, K. Seufert, A. P. Seitsonen, J. Hutter, K. Diller, J. I. Urgel, H. Sachdev, J. V. Barth and W. Auwarter, *ACS Nano*, 2014, **8**, 430-442.
55. M. Schwarz, A. Riss, M. Garnica, J. Ducke, P. S. Deimel, D. A. Duncan, P. K. Thakur, T. L. Lee, A. P. Seitsonen, J. V. Barth, F. Allegretti and W. Auwarter, *ACS Nano*, 2017, **11**, 9151-9161.
56. Q. Li, X. Zou, M. Liu, J. Sun, Y. Gao, Y. Qi, X. Zhou, B. I. Yakobson, Y. Zhang and Z. Liu, *Nano Lett*, 2015, **15**, 5804-5810.
57. J. I. Urgel, M. Schwarz, M. Garnica, D. Stassen, D. Bonifazi, D. Ecija, J. V. Barth and W. Auwarter, *J Am Chem Soc*, 2015, **137**, 2420-2423.
58. P. R. Kidambi, R. Blume, J. Kling, J. B. Wagner, C. Baehtz, R. S. Weatherup, R. Schloegl, B. C. Bayer and S. Hofmann, *Chem Mater*, 2014, **26**, 6380-6392.
59. W. Tress, *Organic Solar Cells*, Springer2014.
60. A. M. Saleh, S. M. Hraibat, R. M. L. Kitaneh, M. M. Abu-Samreh and S. M. Musameh, *Journal of Semiconductors*, 2012, **33**, 082002.
61. A. Laturia, M. L. Van de Put and W. G. Vandenberghe, *npj 2D Materials and Applications*, 2018, **2**, 6.
62. Y. J. Zheng, Y. L. Huang, Y. F. Chenp, W. J. Zhao, G. Eda, C. D. Spataru, W. J. Zhang, Y. H. Chang, L. J. Li, D. Z. Chi, S. Y. Quek and A. T. S. Wee, *ACS Nano*, 2016, **10**, 2476-2484.
63. S. Ossicini, C. M. Bertoni and P. Gies, *Europhysics Letters (EPL)*, 1986, **1**, 661-667.
64. P. Puschnig, P. Amiri and C. Draxl, *Phys. Rev. B*, 2012, **86**, 085107.
65. C. Brülke, T. Heepenstrick, N. Humberg, I. Krieger, M. Sokolowski, S. Weiß, F. S. Tautz and S. Soubatch, *J Phys Chem C*, 2017, **121**, 23964-23973.
66. M. Takada and H. Tada, *Japanese Journal of Applied Physics*, 2005, **44**, 5332-5335.
67. A. Kühnle, *Current Opinion in Colloid & Interface Science*, 2009, **14**, 157-168.
68. P. Amsalem, G. Heimel and N. Koch, in *Encyclopedia of Interfacial Chemistry*, Elsevier2018, pp. 50-67.
69. T. Frederiksen, K. J. Franke, A. Arnau, G. Schulze, J. I. Pascual and N. Lorente, *Phys. Rev. B*, 2008, **78**, 233401.
70. N. Koch, A. Vollmer, S. Duhm, Y. Sakamoto and T. Suzuki, *Advanced Materials*, 2007, **19**, 112-116.
71. K. A. Cochrane, A. Schiffrin, T. S. Roussy, M. Capsoni and S. A. Burke, *Nat Commun*, 2015, **6**, 8312.

72. J. Gómez Díaz, Y. Ding, R. Koitz, A. P. Seitsonen, M. Iannuzzi and J. Hutter, *Theoretical Chemistry Accounts*, 2013, **132**, 1350.
73. R. Koitz, A. P. Seitsonen, M. Iannuzzi and J. Hutter, *Nanoscale*, 2013, **5**, 5589-5595.
74. Y.-L. Wang, J. Ren, C.-L. Song, Y.-P. Jiang, L.-L. Wang, K. He, X. Chen, J.-F. Jia, S. Meng, E. Kaxiras, Q.-K. Xue and X.-C. Ma, *Phys. Rev. B*, 2010, **82**, 245420.
75. J. Ren, S. Meng, Y. L. Wang, X. C. Ma, Q. K. Xue and E. Kaxiras, *J Chem Phys*, 2011, **134**, 194706.
76. Y. Zhang, Y. Luo, Y. Zhang, Y. J. Yu, Y. M. Kuang, L. Zhang, Q. S. Meng, Y. Luo, J. L. Yang, Z. C. Dong and J. G. Hou, *Nature*, 2016, **531**, 623-627.
77. L. Liu, T. Dienel, R. Widmer and O. Groning, *ACS Nano*, 2015, **9**, 10125-10132.
78. N. A. Pradhan, N. Liu and W. Ho, *J Phys Chem B*, 2005, **109**, 8513-8518.
79. G. Heimel, I. Salzmann, S. Duhm and N. Koch, *Chemistry of Materials*, 2011, **23**, 359-377.
80. M. Schwarze, W. Tress, B. Beyer, F. Gao, R. Scholz, C. Poelking, K. Ortstein, A. A. Gunther, D. Kasemann, D. Andrienko and K. Leo, *Science*, 2016, **352**, 1446-1449.
81. P. K. Sahoo, S. Memaran, Y. Xin, L. Balicas and H. R. Gutierrez, *Nature*, 2018, **553**, 63.
82. V. O. Ozcelik, J. G. Azadani, C. Yang, S. J. Koester and T. Low, *Phys. Rev. B*, 2016, **94**, 035125.
83. C. D. Zhang, M. Y. Li, J. Tersoff, Y. M. Han, Y. S. Su, L. J. Li, D. A. Muller and C. K. Shih, *Nat Nanotechnol*, 2018, **13**, 152.
84. W. Chen, S. Chen, S. Chen, Y. Li Huang, H. Huang, D. C. Qi, X. Y. Gao, J. Ma and A. T. S. Wee, *Journal of Applied Physics*, 2009, **106**, 064910.
85. R. Schlesinger, in *Energy-Level Control at Hybrid Inorganic/Organic Semiconductor Interfaces*2017, ch. Chapter 2, pp. 7-45.
86. I. G. Hill, A. Kahn, Z. G. Soos and J. R. A. Pascal, *Chemical Physics Letters*, 2000, **327**, 181-188.
87. L. Glasser, *Inorg Chem*, 2012, **51**, 2420-2424.
88. E. I. Izgorodina, U. L. Bernard, P. M. Dean, J. M. Pringle and D. R. MacFarlane, *Crystal Growth & Design*, 2009, **9**, 4834-4839.
89. S. Sharifzadeh, A. Biller, L. Kronik and J. B. Neaton, *Phys. Rev. B*, 2012, **85**, 125307.

A weakly interacting substrate can significantly perturb the intermolecular charge transfer thus properties of donor-acceptor molecular assemblies via interfacial coupling.

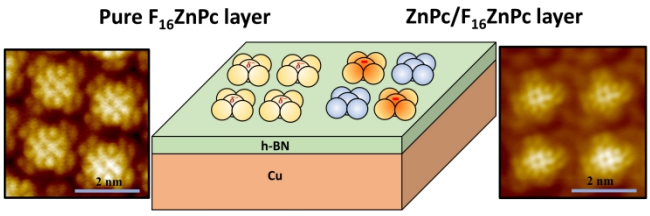

338x190mm (300 x 300 DPI)